# High-order finite elements applied to structural elastic problems

Marco L. Bittencourt, Thais G. Vazquez
*Departamento de Projeto Mecânico, Faculdade de Engenharia Mecânica, Universidade Estadual de Campinas, Campinas, SP – Brazil*

Alberto Costa Nogueira Jr.
*Thorus Scisoft Tecnologia da Informação Ltda., Campinas, SP – Brazil*

## Abstract

The main purpose of this paper is to demonstrate the applicability of the high-order Finite Element Methods for non-linear elastic problems using 3D non-structured meshes. Two finite element bases are presented and compared in terms of the conditioning numbers of the local matrices. A Numerical example is used to validate the application of the Spectral/*hp* FEM in the context of structural mechanics.

Keywords: FEM, spectral/HP finite elements, non-linear elasticity.

## 1 Introduction

The quality of the approximation of Boundary Value Problems (BVP) obtained from the application of the Finite Element Method (FEM) depends on the size and shape of the elements, the properties of the approximation space and the regularity of the solution [1, 2]. From the computational point of view, the choice of the basis for the approximation space influences the stability and efficiency of the numerical procedures used to calculate the approximated solution. In general the finite element basis consist of piecewise polynomial functions defined on the elements of the partition which discretizes the problem domain.

Specifically, the $p$-version of the FEM has the following main features [3, 4]: high-order numerical integration; numerical differentiation; appropriate shape functions; geometric mapping for arbitrary domains; global $C_0$ inter-element continuity; degrees of freedom numbering; application of boundary conditions; and post-processing of results. The $p$-shape functions are associated to the topological entities (vertex, edge, face and body) of the elements. In general, these functions are built from one-dimensional Legendre and Chebyshev polynomials [3, 5, 6]. Hierarchical or modal $p$-basis are characterized by the following properties [4]: vertex modes have one magnitude at one vertex and are zero at all other vertices; edges modes have magnitude along one edge and are zero at all other edges

Mechanics of Solids in Brazil 2007, Marcílio Alves & H.S. da Costa Mattos (Editors)
Brazilian Society of Mechanical Sciences and Engineering, ISBN 978-85-85769-30-7

and vertices; face modes have magnitude along one face but are zero along all other faces, edges and vertices. Hierarchy means that high order expansion sets $X_{p+1}$ contains the terms of the lower order expansion sets $X_p$, i.e., $X_p \subset X_{p+1}$. A nodal basis denotes a non-hierarchical expansion which is associated with a set of nodal points and generally based upon Lagrange polynomials.

Many $p$-shape functions have been presented in the literature [3, 7–16].

Sherwin & Karniadakis [12] presented hierarchical shape functions for triangles and tetrahedra based on collapsed cartesian coordinates, tensorial product, Jacobi orthogonal polynomials and exact numerical integration using tensor product of one-dimensional Gauss-Jacobi quadrature [4]. The collapsed coordinate systems for triangles and tetrahedra are obtained from the cartesian coordinate systems defined on quadrilaterals and hexahedra, respectively.

A fully tensorial-based procedure to construct nodal and modal shape functions for triangles and tetrahedral in barycentric coordinates was presented in [16]. Due to the use of tensorial product, the modal functions have a natural global $C^0$ inter-element continuity. A unified approach to construct $h$- and $p$-shape functions for quadrilaterals, hexahedral, triangles and tetrahedral based on the tensorial product of one-dimensional bases is in [17]. The approach uses indices to denote the one-dimensional polynomials in each tensorization direction. The appropriate manipulation of the indices allows the construction of hierarchical or non-hierarchial and inter-element continuous or non-continuous bases. In addition, a new tensorial basis for triangles is defined aiming to improve the sparsity profiles of the local finite element matrices. The use of tensorial based construction has advantages as the manipulation of only one-dimensional polynomials and their derivatives, better computational performance and simplified implementation of parallel procedures and use of one-dimensional integration rules [16].

The purpose of this paper is to compare the Spectral/*hp* FEM [4], originally developed to CFD, and the shape functions developed [17] for the Laplace operator. After that the Spectral/*hp* FEM is applied to a non-linear elastic problem. The paper is organized as follows. First brief reviews of the Spectral/*hp* FEM and the shape functions given [17] are presented. Comparisons for the Laplace operator is then considered. Finally, results obtained from the application to Spectral/*hp* FEM to a non-linear elasticity problems are presented.

## 2 The Spectral/*hp* Finite Element Method

The Spectral/*hp* FEM uses collapsed coordinate systems to define the shape functions for triangles and tetrahedra. Figure 1 illustrates the procedure to obtain the triangle $T^2 = \{(\xi, \eta) \mid -1 \leq \xi, \eta; \xi + \eta \leq 0\}$ from the square $R^2 = \{(a, b) \mid -1 \leq a, b \leq 1\}$. This transformation allows the use of tensorial product to write the shape functions for triangles. Due to the rational nature of the transformation $(a, b) \longmapsto (\xi, \eta)$ ( $a = \frac{1+\xi}{1-\eta} - 1$), additional terms are included in the local expressions of the shape functions in the coordinates $(a, b)$ to obtain polynomial basis in the local triangular and quadrangular domains. Figure 2 shows the analogous 3-steps transformation to obtain the local tetrahedron $T^3$ from the hexahedron $R^3$ [4, 12].

Local and global operations are defined for the Spectral/*hp* FEM. The local operations are related to the numerical integration, numerical differentiation and the local-global mapping of the shape functions. Connectivity manipulation and degree of freedom numbering are the main global operations.

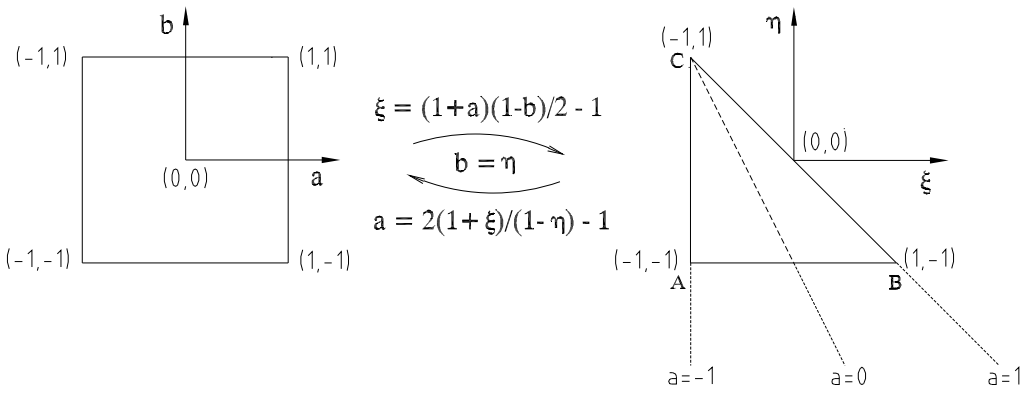


Figure 1: Mapping between quadrilateral and triangular domains [12].

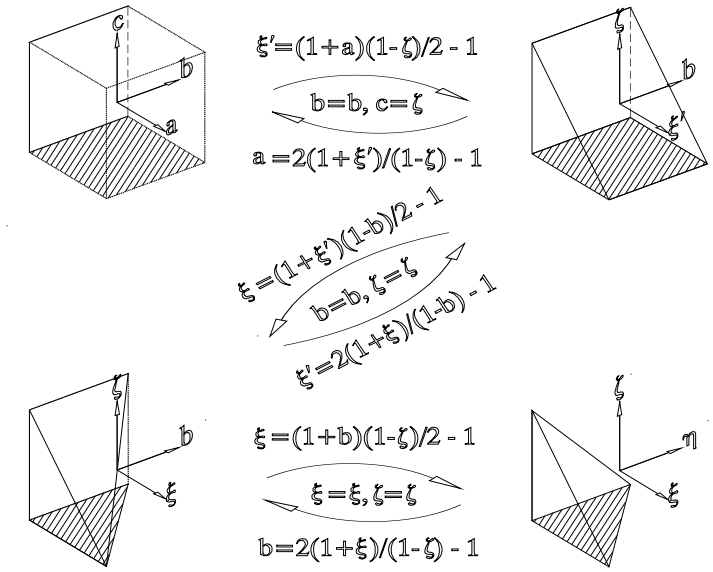


Figure 2: Mapping between hexahedron and tetrahedron domains [12].

Aspects of the numerical integration and differentiation are discussed here briefly. Detailed analysis of the local and global operations, and the appropriate application of boundary conditions, are presented in [4].

The numerical integration in the tetrahedron domain $T^3 = \{(\xi,\eta,\zeta) \mid -1 \leq \xi,\eta,\zeta; \xi+\eta+\zeta \leq -1\}$ uses the collapsed transformation illustrated in Figure 2 which are expressed by the following relations

$$a = 2\frac{(1+\xi)}{(-\eta-\zeta)} - 1, \quad b = 2\frac{(1+\eta)}{(1-\zeta)} - 1, \quad c = \zeta, \tag{1}$$

For the linear and non-linear elasticity problems, the following general expression has to be integrated

$$\int_{T^3} u(\xi,\eta,\zeta)d\xi d\eta d\zeta = \int_{-1}^{1}\int_{-1}^{1}\int_{-1}^{1} u(a,b,c)Jdadbdc\,, \tag{2}$$

where the Jacobian $J$ of the $R^3 \longrightarrow T^3$ transformation is given by

$$J = \frac{\partial(\xi,\eta,\zeta)}{\partial(a,b,c)} = \left(\frac{1-b}{2}\right)\left(\frac{1-c}{2}\right)^2. \tag{3}$$

The numerical integration of (2) from the tensorial product of one-dimensional quadrature rules is

$$\begin{aligned}&\int_{-1}^{1}\int_{-1}^{1}\int_{-1}^{1} u(a,b,c)\left(\frac{1-b}{2}\right)\left(\frac{1-c}{2}\right)^2 dadbdc\\ &= \sum_{i=0}^{Q_1-1} w_i \left\{ \sum_{j=0}^{Q_2-1} w_j \left\{ \sum_{k=0}^{Q_3-1} w_k u(a_i,b_j,c_k)\left(\frac{1-b_j}{2}\right)\left(\frac{1-c_k}{2}\right)^2 \right\} \right\},\end{aligned} \tag{4}$$

where $a_i, b_j$ and $c_k$ are tensorial-based coordinates of the $Q_1, Q_2$ and $Q_3$ quadrature points in each spatial direction $a$, $b$ and $c$, respectively; $w_i, w_j$ and $w_k$ are the respective weights of the Gauss quadrature.

The Gauss-Jacobi quadrature is defined by [4]

$$\int_{-1}^{1}(1-z)^\alpha(1+z)^\beta f(z)dz = \sum_{i=0}^{Q-1} w_i^{\alpha,\beta} f(z_i^{\alpha,\beta}), \tag{5}$$

where $w_i^{\alpha,\beta}$ and $z_i^{\alpha,\beta}$ are the weights and coordinates of the integration points for an appropriate selection of the weights $\alpha$ and $\beta$ of the Jacobi polynomial. For $\alpha = \beta = 0$, the Gauss-Legendre quadrature is obtained. The boundary points of the domain may be included in the numerical integration when using the Gauss-Jacobi quadrature with Lobatto and Radau distributions of points [4].

Based on the previous definition, the number of integration points for the consistent integration of (4) may be reduced with the inclusion of the Jacobian terms in the weights. For that purpose, ($\alpha = 0$,

$\beta = 0$), ($\alpha = 1$, $\beta = 0$) and ($\alpha = 2$, $\beta = 0$) are selected, respectively, in the directions $a$, $b$ and $c$. The integration on $T^3$ given in (4) may be written as

$$\int_{-1}^{1}\int_{-1}^{1}\int_{-1}^{1} u(a,b,c)\left(\frac{1-b}{2}\right)\left(\frac{1-c}{2}\right)^2 dadbdc$$
$$= \sum_{i=0}^{Q_1-1} w_i^{0,0}\left\{\sum_{j=0}^{Q_2-1}\hat{w}_j^{1,0}\left\{\sum_{k=0}^{Q_3-1}\hat{w}_k^{2,0}u(a_i^{0,0},b_j^{1,0},c_k^{2,0})\right\}\right\}, \tag{6}$$

where

$$\hat{w}_j^{1,0} = \frac{w_j^{1,0}}{2} \text{ and } \hat{w}_k^{2,0} = \frac{w_k^{2,0}}{4}. \tag{7}$$

The Gauss-Radau distribution is used in the $\eta, \zeta$ directions while the Gauss-Lobatto points are considered for the $\xi$ direction as illustrated in Figure 3. This selection avoids multiple points on the vertices ($\xi = -1$, $\eta = -1$, $\zeta = 1$) and ($\xi = -1$, $\eta = 1$, $\zeta = 1$) and along the edge that connects these vertices. Therefore, the calculation on the singular points of the collapsed transformation is avoided. Although numerical perturbations would be expected when using singular integration points, [4] gave a theoretical proof demonstrating the boundness of the collapsed transformation over the singular points.

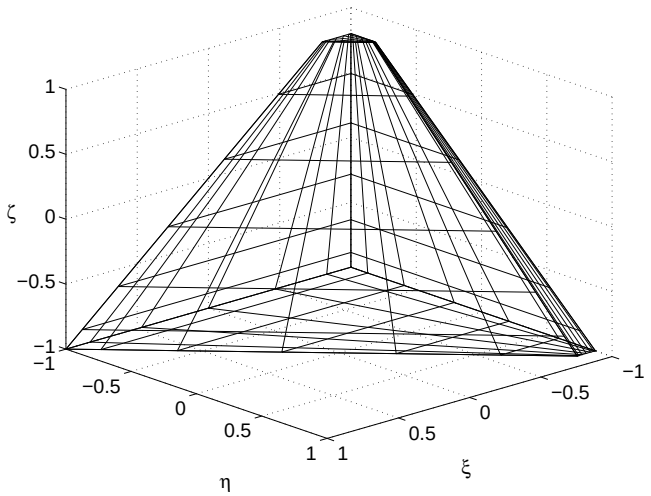


Figure 3: Quadrature points for the local tetrahedron $T^3$ with $Q_1 = Q_2 = Q_3 = 7$ and Gauss-Lobatto points in the $\xi$-direction and Gauss-Radau points in the $\eta$ and $\zeta$-directions [4].

The differential operators of the linear and non-linear elasticity problems are applied to the shape functions of the approximation space and evaluated on the integration points for each finite element of

the mesh. The collocation differentiation may be used to calculate the derivatives of the shape functions on the integration points [4]. It is based on the representation of arbitrary polynomial functions by Lagrange polynomials defined on the quadrature coordinates. The representation is a simple change of basis for the same polynomial space. Based on that, the local polynomial approximation for a one-dimensional function $u(\xi)$ is written as

$$u(\xi) = \sum_{p=0}^{P_1} \hat{u}_p \phi_p(\xi) = \sum_{p=0}^{P_1} u_p h_p(\xi) \tag{8}$$

where $\phi_p(\xi)$ are the interpolation functions of order $\leq P_1$, $h_p(\xi)$ are the Lagrange polynomials defined on the $P_1+1$ integration points and $\hat{u}_p$ and $u_p$ are the coefficients of the approximation in the original and transformed basis, respectively. Due to the collocation property of the Lagrange polynomials (i.e., $h_i(\xi_j) = \delta_{ij}$), the coefficients $u_p$ are the values of the approximated function on the integration points, i.e., $u_p = u(\xi_p)$. Therefore, it is possible to express the derivative of the approximated function as

$$\frac{\partial u}{\partial \xi}(\xi) = \sum_{p=0}^{P_1} u_p \frac{\partial h_p}{\partial \xi}(\xi) = \sum_{p=0}^{P_1} u(\xi_p) \frac{\partial h_p}{\partial \xi}(\xi). \tag{9}$$

For the reference element $T^3$, which is mapped from the hexahedron $R^3$, the polynomial expansion of the function $u(a,b,c)$ in terms of Lagrange polynomials in the tensorial coordinates $a, b$ and $c$ is

$$u(a,b,c) = \sum_{p,q,r=0}^{P_1,P_2,P_3} \hat{u}_{pqr} \psi_{pqr}(a,b,c) = \sum_{p=0}^{P_1} \sum_{q=0}^{P_2} \sum_{r=0}^{P_3} u_{pqr} h_p(a) h_q(b) h_r(c), \tag{10}$$

where $\psi_{pqr}(a,b,c) = \phi_{pqr}(\xi,\eta,\zeta)$ are the basis functions represented in the tensorized space $(a,b,c)$ and $h_j$ (for $j = p,q,r$) are the Lagrange polynomials of order $P_i$ $(i = 1,2,3)$.

Analogously to equation (9), the partial derivatives of the approximated function are

$$\frac{\partial u}{\partial a}(a,b,c) = \sum_{p=0}^{P_1} \sum_{q=0}^{P_2} \sum_{r=0}^{P_3} u_{pqr} \frac{\partial h_p(a)}{\partial a} h_q(b) h_r(c), \tag{11}$$

$$\frac{\partial u}{\partial b}(a,b,c) = \sum_{p=0}^{P_1} \sum_{q=0}^{P_2} \sum_{r=0}^{P_3} u_{pqr} h_p(a) \frac{\partial h_q(b)}{\partial b} h_r(c), \tag{12}$$

$$\frac{\partial u}{\partial c}(a,b,c) = \sum_{p=0}^{P_1} \sum_{q=0}^{P_2} \sum_{r=0}^{P_3} u_{pqr} h_p(a) h_q(b) \frac{\partial h_r(c)}{\partial c}. \tag{13}$$

The evaluation of the previous expressions on the integration points using the collocation property of the Lagrange polynomials gives

$$\frac{\partial u}{\partial a}(a_i, b_j, c_k) = \sum_{p=0}^{P_1} u_{pjk} \left. \frac{\partial h_p(a)}{\partial a} \right|_{a_i}, \tag{14}$$

$$\frac{\partial u}{\partial b}(a_i, b_j, c_k) = \sum_{q=0}^{P_2} u_{iqk} \left. \frac{\partial h_q(b)}{\partial b} \right|_{b_j}, \tag{15}$$

$$\frac{\partial u}{\partial c}(a_i, b_j, c_k) = \sum_{r=0}^{P_3} u_{ijr} \left. \frac{\partial h_r(c)}{\partial c} \right|_{c_k}. \tag{16}$$

The procedures for the collocation differentiation, which result from the evaluation of the derivatives of Lagrange polynomials, are discussed in [4] and based on the distribution of points for the Gauss-Jacobi, Gauss-Legendre, Gauss-Radau and Gauss-Lobatto quadratures.

From expressions (14) to (16), the chain rule is applied to obtain the local partial derivatives with respect to the cartesian coordinates $(\xi, \eta, \zeta)$ of the reference element $T^3$, i.e.,

$$\nabla = \begin{pmatrix} \dfrac{\partial}{\partial \xi} \\ \dfrac{\partial}{\partial \eta} \\ \dfrac{\partial}{\partial \zeta} \end{pmatrix} = \begin{pmatrix} \dfrac{4}{(1-b)(1-c)} \dfrac{\partial}{\partial a} \\ \dfrac{2(1+a)}{(1-b)(1-c)} \dfrac{\partial}{\partial a} + \dfrac{2}{(1-c)} \dfrac{\partial}{\partial b} \\ \dfrac{2(1+a)}{(1-b)(1-c)} \dfrac{\partial}{\partial a} + \dfrac{(1+b)}{(1-c)} \dfrac{\partial}{\partial b} + \dfrac{\partial}{\partial c} \end{pmatrix}. \tag{17}$$

For the cases $b = 1$ or $c = 1$, the operator $\nabla$ becomes singular. This problem may be avoided using Gauss-Radau quadrature along the $b$ and $c$-directions.

## 3 Fully tensorial bases for triangles and tetrahedra

The shape functions for triangles may be written as the tensorial product of one-dimensional bases expressed in natural coordinates as [17]

$$N_{pqr}(L_1, L_2, L_3) = \phi_p(L_1)\phi_q(L_2)\phi_r(L_3). \tag{18}$$

Generally, $0 \leq p \leq P_1$, $0 \leq q \leq P_2$ and $0 \leq r \leq P_3$ and $P_1$, $P_2$ and $P_3$ are the degrees of the polynomial bases along the area coordinates $L_1$, $L_2$ and $L_3$, respectively.

As indicated in Figure 4, the vertex modes are given by

$$\begin{aligned} N_{P_1 00}(L_1, L_2, L_3) &= \phi_{P_1}(L_1)\phi_0(L_2)\phi_0(L_3), \\ N_{0P_2 0}(L_1, L_2, L_3) &= \phi_0(L_1)\phi_{P_2}(L_2)\phi_0(L_3), \\ N_{00P_3}(L_1, L_2, L_3) &= \phi_0(L_1)\phi_0(L_2)\phi_{P_3}(L_3). \end{aligned} \tag{19}$$

The edge modes ($0 < p, q, r < P$ and $P_1 = P_2 = P$) are

$$\begin{aligned} N_{pq0}(L_1, L_2, L_3) &= \phi_p(L_1)\phi_q(L_2)\phi_0(L_3), \\ N_{p0r}(L_1, L_2, L_3) &= \phi_p(L_1)\phi_0(L_2)\phi_r(L_3), \\ N_{0qr}(L_1, L_2, L_3) &= \phi_0(L_1)\phi_q(L_2)\phi_r(L_3). \end{aligned} \tag{20}$$

Finally, the general expression for the face modes ($0 < p, q, r < P - 1$) is

$$N_{pqr}(L_1, L_2, L_3) = \phi_p(L_1)\phi_q(L_2)\phi_r(L_3). \tag{21}$$

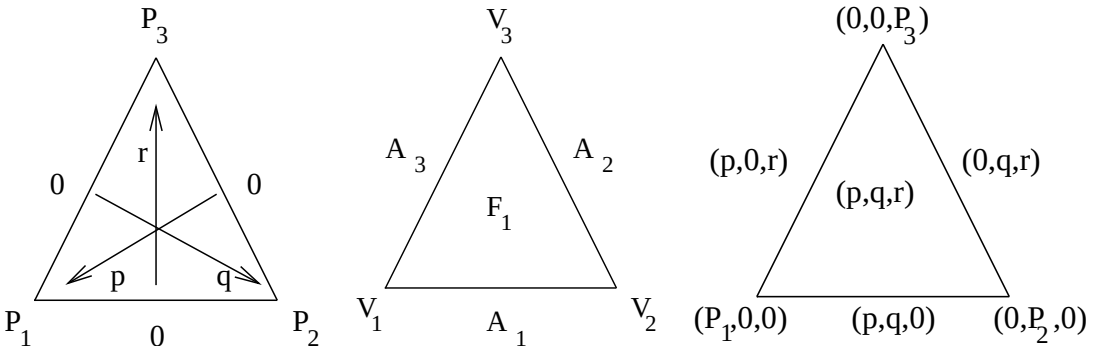


(a) Indices $p$, $q$ and $r$. (b) Topological entities. (c) Entities and indices $p$, $q$ and $r$.

Figure 4: Association of topological entities and indices $p$, $q$, $r$ for triangles.

Hierarchical and non-hierarchical nodal bases may be constructed, respectively, using the following definitions

$$\phi_p(L_1) = \begin{cases} 1 & p = 0 \\ L_1 L_p^{(P_1-2)}(L_1) & 0 < p \leq P_1 \end{cases}, \tag{22}$$

$$\phi_p(L_1) = \begin{cases} 1 & p = 0 \\ L_1 & p = P_1 \\ L_1 L_p^{(P_1-2)} & 0 < p < P_1 \end{cases}. \tag{23}$$

The truncated Lagrange polynomial is defined by [17]

$$L_p^{(P_1-2)}(L_1) = -4 \frac{\prod_{q=1, q\neq p}^{P_1-1} (L_1 - L_{1_q})}{\prod_{q=0, q\neq p}^{P_1} (L_{1_p} - L_{1_q})}.$$

Modal basis for triangles are obtained using

$$\phi_p(L_1) = \begin{cases} 1 & p = 0 \\ L_1 & p = P_1 \\ 2L_1 P_{p-1}^{\alpha_1,\beta_1}(2L_1 - 1) & 0 < p < P_1 \end{cases} . \tag{24}$$

Similar expressions are defined for the $L_2$ and $L_3$ directions.

The extension for tetrahedra is direct and the shape functions are given by

$$N_{pqrs}(L_1, L_2, L_3, L_4) = \phi_p(L_1)\phi_q(L_2)\phi_r(L_3)\phi_s(L_4), \tag{25}$$

The indices $p, q, r, s$ are indicated in Figure 5.

Due to their tensorial nature, the non-hierarchical bases obtained using the previous procedures have a natural $C_0$-continuity [17]. In addition, very efficient tensorial based integration rules may be used.

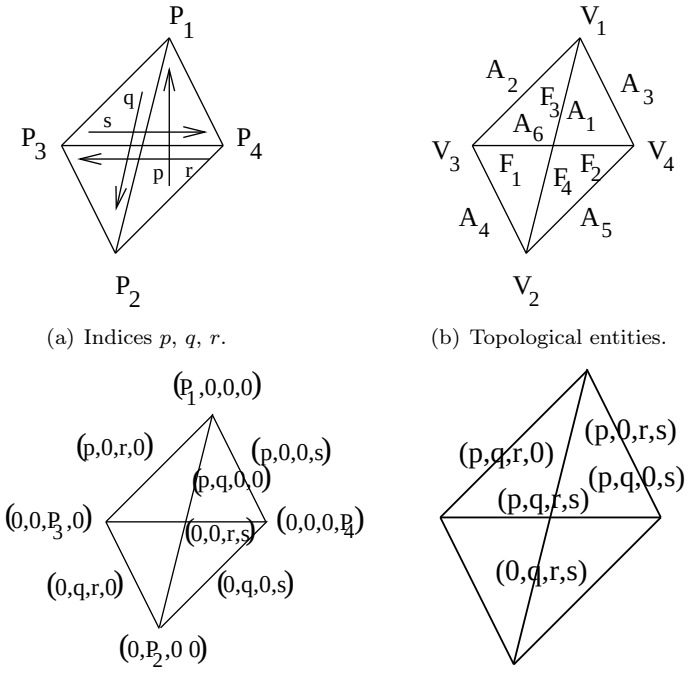


(a) Indices $p$, $q$, $r$.

(b) Topological entities.

(c) Vertices and edges.

(d) Faces and volume

Figure 5: Association of topological entities and indices $p$, $q$, $r$, $s$ for tetrahedra.

## 4 Results

### 4.1 Comparison of the bases

In this section, the Sherwin-Karniadakis and the fully tensorial bases for triangles are compared in terms of the condition numbers of the local mass and stiffness matrices for the Laplace operator. The results are shown in Figure 6 for one local element with and without the Schur's complement. Figure 7 shows the conditioning for a mesh of eight elements for the tensorial basis, with and without the Schur's complement. For the tensorial basis, $\alpha = 0$ and $\beta = 2$ were used due to the best conditioning of the element matrices.

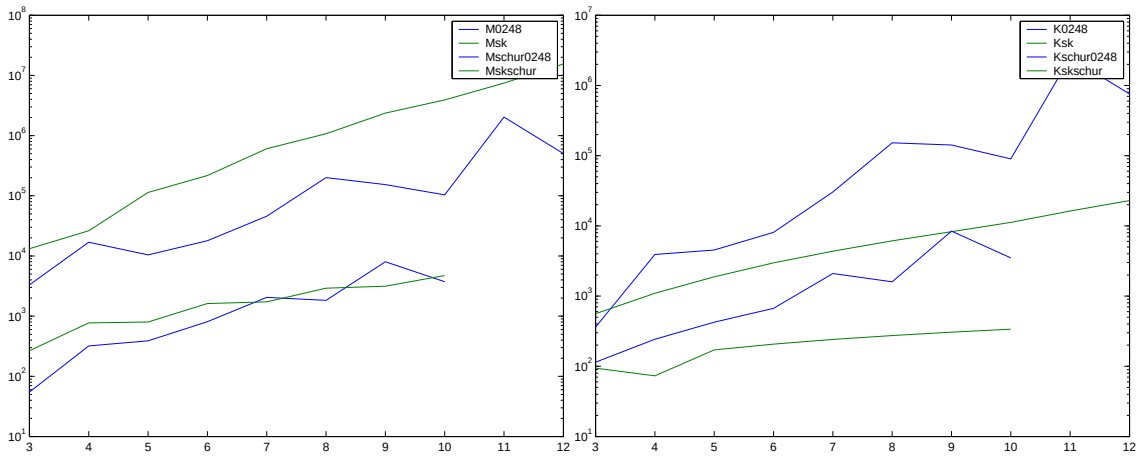


(a) Mass. (b) Stiffness.

Figure 6: Condition numbers of the mass and stiffness matrices for the Sherwin (sk) and Bittencourt bases.

The behavior of the tensorial basis is similar to the Sherwin-Karniadakis basis, but for the stiffness matrix the last basis is superior for non-distorted elements. The condition numbers for Basis 1 with odd degrees increase remarkably.

### 4.2 Non-linear elasticity

The Spectral/*hp* FEM will be applied to the problem of large deformation of a cantilever beam submitted to its own weight and a constant surface load [2]. The mesh used of 23 tetrahedra, the boundary conditions and surface load are illustrated in Figure 8. The dimensions of the beam are $c = 3.0\,m \times l = 0.3\,m \times h = 0.05\,m$. The material properties are $\rho = 250.0\ kg/m^3$, $E = 4.0 \times 10^8\ N/m^2$

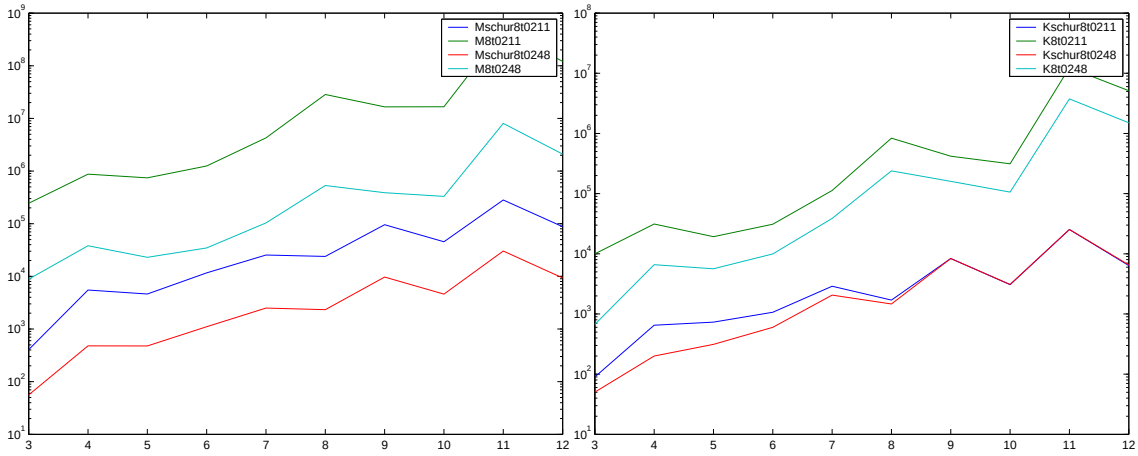


(a) Mass. (b) Stiffness.

Figure 7: Condition numbers of the mass and stiffness matrices for a mesh of 8 triangles.

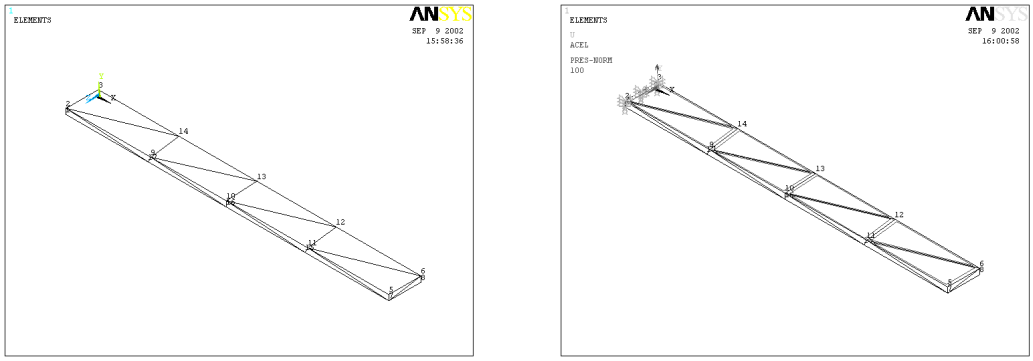


(a) Mesh with 23 elements. (b) Boundary conditions.

Figure 8: Non-linear cantilever beam.

and $\nu = 0.3$. The surface load intensity is $100.0\,N/m^2$ and applied in the negative $y$-direction. The solutions were obtained for $p = 1, \ldots, 8$ using the Newton-Raphson method with one load step. The energy stop criterion in the Euclidian norm were used with $10^{-4}$ precision. The results are compared for one node of the mesh with the non-linear formulation of the ANSYS software based on the $h$-version and taking the equivalent numbers of degrees of freedom for the two formulations.

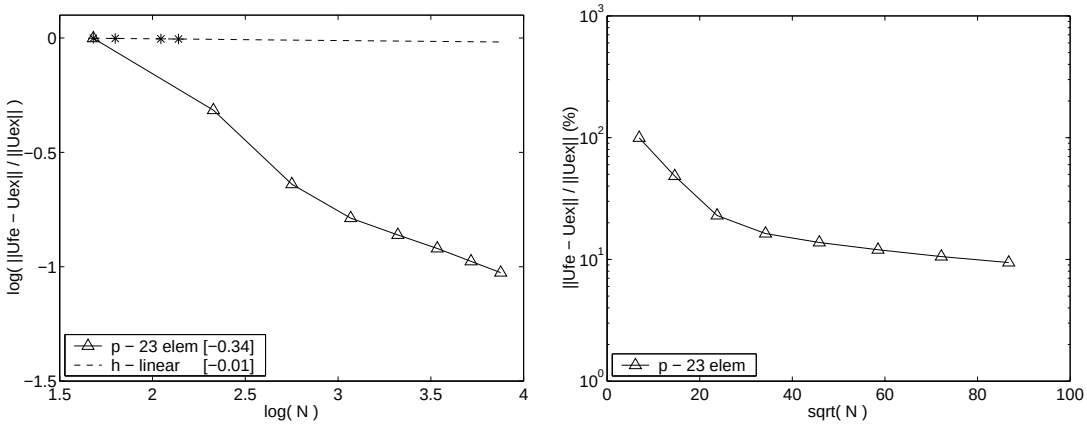


(a) Relative error vs. number of dofs. (b) Percentual relative error vs. $\sqrt{}$number of dofs.

Figure 9: Error behaviour for the non-linear cantilever beam.

Figures 9(a) and 9(b) show the convergence behaviour of the solutions in the non-linear cantilever beam when the approximation space is refined for $p = 1, \ldots, 8$. The convergence is indicated, respectively, in terms of the logarithmic and percentual of the relative error in the energy norm versus the number of degrees of freedom. Figure 9(a) also shows the comparison of the relative errors for the $h$ and $p$ versions of FEM. The results for the $h$-version were extrapolated based on the solutions calculated for meshes of 23, 33, 64 and 108 elements.

As in the linear case, it may be observed from Figure 9(a) that the $p$-version has an exponential convergence rate for the non-linear cantilever beam. The rate of convergence of the $p$-version is very superior when compared with the results obtained for $h$-version. For non-linear problems, the larger stiffness produced by the linear Lagrange elements is more critical when compared to the linear case.

The estimate of the energy of the exact solution for the mesh with 23 elements using the *a-posteriori* estimate given [3] is

$$\Pi(u) \approx 21.19735351. \tag{26}$$

For the mesh with 23 elements illustrated in Figure 8(a) and polynomial order $p = 5$, Figure 10 shows the behaviour of the non-linear solution obtained with 5 load steps according to the Euclidian norm of the load, displacement and energy criteria of the Newton-Rhapson procedure [18]. It may be observed that the convergence criteria are not absolutely equivalent in terms of the norms of their respective expressions used to measure convergence. The energy criterion has an intermediate behaviour and is situated between the limits of the displacement and load criteria.

Figure 11 shows the displacements in the $y$-direction for one node of the mesh obtained from the linear and non-linear models. Due to the non-linear stiffness, the displacement at the end of each load step is lower than that of the linear case.

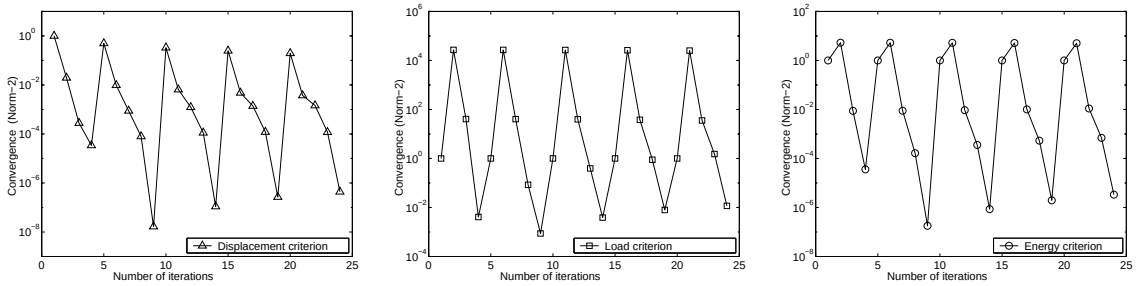


(a) Displacement criterion. (b) Load criterion. (c) Energy criterion.

Figure 10: Convergence of Newton-Rhapson iterations for the three convergence criteria versus the total number of iterations and $p = 5$.

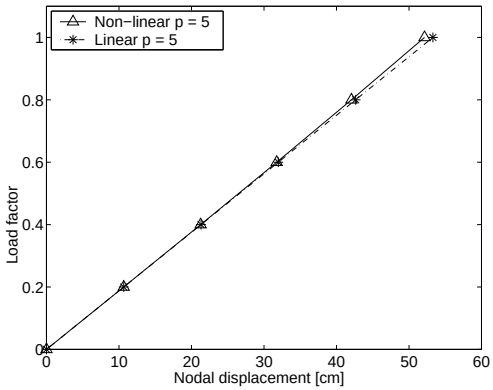


Figure 11: Load steps versus the nodal $y$-displacement for the linear and non-linear models.

Table 1 presents the comparison of the displacement components for one node of the mesh calculated using the ANSYS program and the Spectral/*hp* FEM. Two different meshes were used. The *p*-mesh has 23 tetrahedral and polynomial order $p = 5$. The ANSYS mesh has 303 quadratic tetrahedral. For both meshes, the number of degrees of freedom is 2100. The displacement and load convergence criteria were used simultaneously in the ANSYS program. The precisions were $10^{-3}$ and $10^{-6}$ for the load and displacement convergence criteria, respectively. For the Spectral/*hp* FEM, the energy criterion was used with $10^{-4}$ precision. The results have a reasonable agreement which shows that the Spectral/*hp* Methods are suitable also for non-linear solid mechanic problems.

Table 1: Comparison of the nodal solution for the non-linear cantilever beam obtained from the ANSYS program and the Spectral/*hp* Method.

| | | | | Displacement $\mathbf{u}$ $[m]$ | | |
|---|---|---|---|---|---|---|
| Mesh | DOFs | Node | Formulation | $u_x$ | $u_y$ | $u_z$ |
| h | 2100 | 5 | ANSYS | -0,46644e-01 | -0,52177 | 0,50587e-04 |
| $p = 5$ | 2100 | 5 | Spectral/*hp* | -0,46630e-01 | -0,52143 | -0,13399e-03 |

## 5 Conclusions

Traditionally, high-order methods have been used in fluid mechanics. This paper presented two high-order finite element bases that may be used effectively to problems of solid mechanics. The behavior of the two bases are similar in terms of the conditioning of the local matrices. The fully tensorial basis has been implemented in a C++ software basis and will be applied to impact problems.

### References

[1] Nogueira Jr., A. & Bittencourt, M., Algebraic multigrid schemes for the *p*-version of the finite element method applied to 3D elliptical problems. *Proceedings of the 5th World Congress on Computational Mechanics (WCCM V)*, Technical University of Vienna and IACM: Vienna - Austria, 2002.

[2] Nogueira Jr., A., *Formulação* p *do Método de Elementos Finitos em Problemas de Elasticidade Linear e Não-Linear com Malhas 3D Não-Estruturadas e em Métodos Multigrid Algébricos*. Ph.D. thesis, Faculdade de Engenharia Mecânica, Universidade Estadual de Campinas, 2002.

[3] Szabó, B.A. & Babuška, I., *Finite Element Analysis*. Wiley Interscience: New York, 1991.

[4] Karniadakis, G.E. & Sherwin, S.J., *Spectral/hp Element Methods for CFD*. Oxford University Press: Oxford, 1999.

[5] Vijayakar, S., Busby, H. & Houser, D., Finite element analysis of quasi-prismatic bodies using Chebyshev polynomials. *Int J Num Meth Engrg*, **24**, pp. 1461–1477, 1987.

[6] Devloo, P., Oden, J. & Pattani, P., Shape optimization of structures: A literature survey. *Comput Meth Appl Mech Engrg*, **70**, pp. 203–235, 1988.

[7] Peano, A., *Hierarchies of conforming finite elements*. Master's thesis, Washington University - St. Louis, 1975.

[8] Peano, A., Hierarchies of conforming finite elements for plane elasticity and plate bending. *Computers and Mathematics with Applications*, **2**, pp. 211–224, 1976.

[9] Katz, I., Nodal variables for complete conforming finite elements of arbitrary polynomial order. *Computers and Mathematics with Applications*, **4**, pp. 85–112, 1978.

[10] Rossow, M. & Katz, I., Hierarchical finite elements and precomputed arrays. *Int J Numer Methods Eng*, **12**, pp. 977–999, 1993.

[11] Carnevali, P., Morris, R.B., Tsuji, Y. & Taylor, G., New basis functions and computational procedures for *p*-version finite element analysis. *Int J Numer Methods Engrg*, **36**, pp. 3759–3779, 1993.

[12] Sherwin, S. & Karniadakis, G., A new triangular and tetrahedral basis for high-order (*hp*) finite element methods. *Int J Numer Methods Engrg*, **38**, pp. 3775–3802, 1995.
[13] Webb, J.P. & Abouchakra, R., Hierarchal triangular elements using orthogonal polynomials. *Int J Numer Methods Engrg*, **38**, pp. 245–257, 1995.
[14] Adjerid, S., Aiffa, M. & Flaherty, J., Hierarchical finite element bases for triangular and tetrahedral elements. *Comput Methods Appl Mech Engrg*, **190**, pp. 2925–2941, 2001.
[15] Nogueira Jr., A. & Bittencourt, M., Hierarchical basis functions for the *p*-version of the finite element method (in portuguese). *Revista Internacional de Métodos Numéricos para Cálculo y Diseño en Ingeniería*, **17(1)**, pp. 37–59, 2001.
[16] Bittencourt, M., Fully tensorial nodal and modal shape functions for triangles and tetrahedra. *Int Journal for Numerical Methods in Engineering*, **63**, pp. 1530–1558, 2005.
[17] Bittencourt, M., Vazquez, M. & Vazquez, T., Construction of shape functions for the *h*- and *p*-versions of the fem using tensorial product. *Int Journal for Numerical Methods in Engineering*, 2006. In press.
[18] Bonet, J. & Peraire, J., An alternating digital tree (ADT) algorithim for 3D geometric searching. *International Journal for Numerical Methods in Engineering*, **38**, pp. 3529–3544, 1995.

Mechanics of Solids in Brazil 2007, Marcílio Alves & H.S. da Costa Mattos (Editors)
Brazilian Society of Mechanical Sciences and Engineering, ISBN 978-85-85769-30-7